RSC Advances

ROYAL SOCIETY OF CHEMISTRY

www.rsc.org/advances

Highly scalable production of uniformly-coated superparamagnetic nanoparticles for triggered drug release from alginate hydrogels

Alexandra Teleki[1], *Florian L. Haufe*[1], *Ann M. Hirt*[3], *Sotiris E. Pratsinis*[1], *Georgios A. Sotiriou*[1,2]*

[1]Particle Technology Laboratory, Institute of Process Engineering, Department of Mechanical and Process Engineering, ETH Zurich, Sonneggstrasse 3, CH-8092 Zurich, Switzerland.
[2]Drug Formulation & Delivery, Institute of Pharmaceutical Sciences, Department of Chemistry and Applied Biosciences, ETH Zurich, Vladimir-Prelog-Weg 3, CH-8093 Zurich, Switzerland.
[3]Institute of Geophysics, Department of Earth Sciences, ETH Zurich, Sonneggstrasse 5, CH-8092 Zurich, Switzerland.

15 February 2016

Submitted to:

RSC Advances

*Corresponding author: georgios.sotiriou@pharma.ethz.ch

Table of contents graphic

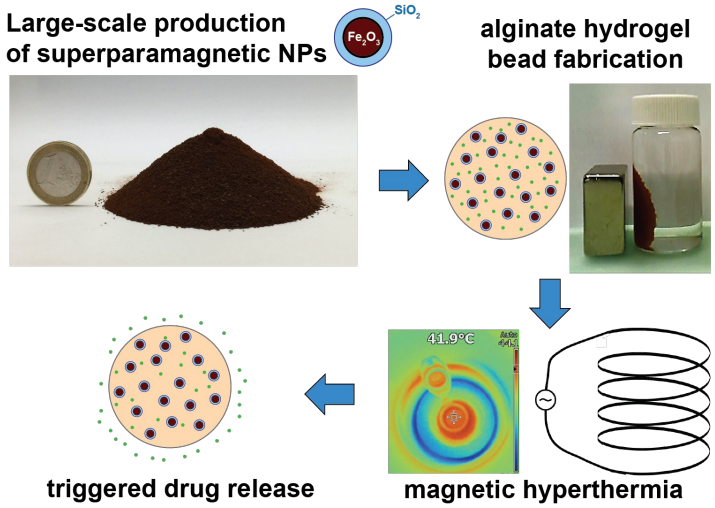

Large-scale production of SiO_2-coated Fe_2O_3 nanoparticles facilitates their incorporation in stimuli-responsive superparamagnetic alginate hydrogel structures with efficient hyperthermia performance and enhanced triggered drug release.

Abstract

Intelligent, on-demand drug administration systems with controlled release kinetics may revolutionize the way diseases are treated. Typically, the release of the therapeutic payload from these systems is activated by stimuli-responsive nanofillers. However, limitations regarding large-scale nanomaterial production and poor reproducibility keep such systems in the labs and away from clinics. Here, we demonstrate the highly scalable and reproducible synthesis of uniform superparamagnetic Fe_2O_3 nanoparticles coated with a nanothin layer of amorphous SiO_2 and evaluate their suitability as stimuli-responsive nanofillers in a drug-loaded biopolymer alginate matrix. The superior colloidal stability of the SiO_2-coated Fe_2O_3 nanoparticles over their uncoated counterparts and their dispersibility in aqueous suspensions facilitates their incorporation in alginate hydrogel microbeads. We examine the hyperthermia performance of such multi-scale particle structures in the presence of alternating magnetic fields and compare the release of dextran (a model biomolecule) in the presence and absence of external stimuli. The enhanced triggered release of dextran in the presence of magnetic fields further highlights the potential of such superparamagnetic SiO_2-coated Fe_2O_3 nanoparticles as a functional transducer in such systems.

Keywords: aerosol nanomanufacturing, core-shell, magnetic fluid hyperthermia, nanomedicine

Introduction

Nanotechnology is rapidly gaining recognition as an integral part of biomedicine with drug delivery being one of the most promising applications.[1] Multifunctional nanoparticles with magnetic and optical properties carefully matched to their respective task have the potential to revolutionize the treatment of complex diseases.[2] In particular, nanoparticles can be fabricated that are sensitive to externally applied physical stimuli such as magnetic fields[3] or laser light.[4] Therefore, they can serve as transducer entities to trigger drug release from tailor-made delivery vehicles.[5] Such vehicles are primarily polymeric matrices offering additional control of drug release due to their tunable degradation properties. Combining the stimuli-responsive nanoparticles with a drug-loaded polymeric microcapsule leads to intelligent, on-demand drug administration systems with controlled release kinetics.[6] This may not only improve the therapeutic efficacy,[7] but also minimizes undesirable side-effects and allows time for spatial targeting.[8] For example, a number of new molecular entities, which were abandoned because of side-effects, could be reconsidered based on these improvements.[1]

One significant barrier, however, to the development and commercialization of novel nanotechnologies for biomedical applications is their economic large-scale production with minimal batch-to-batch variation.[9] For example, the use of iron oxide nanoparticles in clinics for contrast enhancement in magnetic resonance imaging (MRI) has been abandoned due to poor reproducibility resulting from batch-to-batch size variation.[10] The healthcare industry will only adopt nanomanufacturing processes if they are fast, scalable, reproducible and cost-efficient.[11] In fact, the large-scale production of uniform nanomaterials is also very important for their path *towards* commercialization. The required nanomaterial amount is geometrically increased for every single step from *in vitro* cell work, to small animal, to primate and eventual clinical trial testing.[10] Therefore, the suitability of nanomaterials made by scalable methods with high control over their morphology and physicochemical properties for such bioapplications is crucial for their successful implementation.[10,12]

Iron oxide nanoparticles are one of the most studied material for biomedical applications due to their magnetic properties and high biocompatibility.[13] Magnetic nanoparticles have been intensively studied for biomedical applications showing great potential (review [14] and referenced therein). For very small crystal size, iron oxides exhibit the so-called superparamagnetic behavior,[13] a feature combining high magnetization with no coercivity, hence no permanent magnetization. Such superparamagnetic nanoparticles exhibit

potential in therapeutic applications due to their ability to transform the energy of an alternating magnetic field (AMF) to thermal energy by magnetic relaxation through Brownian and Neel mechanisms,[15] a process that is often called magnetic fluid hyperthermia.[16] Therefore, aqueous suspensions at relatively high nanoparticle concentrations (g/L), *i.e.* ferrofluids,[17] also increase their temperature in the presence of an external AMF. This property renders such materials interesting for the non- or minimally-invasive selective destruction of cancer cells upon the nanoparticle localization at a tumor site.[18] Building upon the attractive properties of iron oxide nanoparticles, multifunctional iron oxide-based hybrid nanoaggregates have been made with silver (Ag)[19] and gold (Au)[20] nanoparticles to allow the optical detection and plasmonic photothermal excitation of the hybrid complexes.

Typically, nanoparticles are either coated[21] or modified with surface ligands such as citrate ions[22] to obtain aqueous dispersibility, stability and biocompatibility that are required typically for drug delivery applications. Among the most common coatings are polymers, proteins, functional silanes (e.g. amine, carboxyl, epoxy) and amorphous silica (SiO_2).[21,23] The drug payload can be directly integrated in this coating.[24-25] However, to increase the drug loading capacity, the coated nanoparticles are often embedded in a polymer matrix structure which contains the relevant drug.[26] Among the polymers used as a matrix is alginate, a natural polysaccharide harvested from brown algae.[27] Alginates qualify as part of a drug delivery system because of their biocompatibility, low toxicity, relatively low cost and controlled gelation,[28] properties that render them attractive for bioapplications till today.[29-30] Most commonly, alginate precursors are prepared as aqueous solution and subsequently gelled by ionic cross-linking using divalent calcium cations (Ca^{2+}).[31] Alginate microbeads containing superparamagnetic nanoparticles exhibit enhanced drug release in the presence of an AMF. This has been observed for anticancer drugs[22] and insulin[32] with up to 2-fold enhancements. Other hydrogel systems based on thermally-responsive polymers have also been suggested in the literature achieving triggered drug release.[33-34]

This study focuses on the synthesis of uniform SiO_2-coated Fe_2O_3 nanoparticles by flame spray pyrolysis (FSP),[23] a technique with proven scalability[35] and production rate from gram-level lab-scale to pilot plant reactors with up to 10 metric tons annually.[36] We evaluate the nanoparticles potential as stimuli-responsive nanofillers in a multi-scale composite structure consisting of alginate microbeads and a model biomolecule. The physicochemical[23] as well as magnetic properties[37-38] of such flame-made SiO_2-coated Fe_2O_3 nanoparticles have already been characterized in detail. Here, we focus on the characteristics of the hybrid

alginate hydrogel beads and evaluate their potential in magnetic fluid hyperthermia in the presence of an external AMF. Finally, we investigate the cumulative biomolecule release in the presence and absence of the external stimuli aiming to achieve a triggered enhanced release.

Materials and Methods

Large-scale nanoparticle synthesis and characterization

The FSP reactor was set up and operated following Teleki et al.[23] Two different types of magnetic nanoparticles were synthesized, one with a nominal SiO_2 coating of 23 wt% and another one without coating. In brief, as precursor solution, iron(III) acetylacetonate ($Fe(acac)_3$, Fluka, purity ≥97%) in xylene (Sigma-Aldrich, purity ≥ 98.5 %) and acetonitrile (Sigma-Aldrich, purity ≥ 99.5 %) (3:1 volume ratio) with a total iron concentration of 0.34 M was fed at 5 mL/min (Lambda Vit-Fit syringe pump). The precursor feed was dispersed by 5 L/min O_2 (Pan Gas, purity ≥ 99%) and the resulting solution spray was ignited by a premixed ring-shaped flame consisting of 1.5 L/min CH_4 and 3.2 L/min O_2. At the nozzle tip, the pressure drop was kept constant at 1.5 bar. The spray flame was sheathed by 40 L/min O_2 flowing through the outermost sinter metal plate at the FSP burner. A 20 cm long quartz glass tube enclosed the FSP reactor. For the *in-situ* SiO_2 coating, a stream of N_2 carrying hexamethyldisiloxane (HMDSO, Aldrich, purity ≥ 98%) was introduced from a bubbler at 10 ˚C through a metal torus pipe ring[39] along with additional N_2 as mixing gas (total N_2 flow rate of 15 L/min). To achieve the targeted silica-content of 23 wt% in the final product, the stream of N_2 through the HMDSO bubbler was adjusted to 0.45 L/min. For the synthesis of uncoated particles, pure N_2 mixing gas was fed through the ring as above. Another 30 cm long quartz glass tube mounted above that ring facilitated the SiO_2 coating of nano-Fe_2O_3 prior to collection on glass fiber filter downstream.[40]

The crystallinity of the powder obtained from FSP was analyzed by X-ray diffraction (XRD, Bruker AXS D8 Advance, Cu-anode) and the specific surface area by N_2 adsorption (Micromeritics Tristar II Plus) at 77 K. The crystallite size of particles was calculated based on the interval $2\theta = [34.7^\circ, 36.7^\circ]$ corresponding to the main diffraction peak of the maghemite structure using TOPAS3 software. Particles were dispersed in 10 mL of Milli-Q water by ultrasonication (Sonics VibraCell) for 10 s to 1800 s while submerged in a cooled water bath. Ultrasound energy was delivered in a pulsed manner (30 s ON / 1 s OFF) and the power output was kept constant at 361 W/L corresponding to 80 % amplitude. Dynamic light scattering (DLS, Malvern Zetasizer Nano series) was used to measure size distributions after ultrasonication and assess the

dispersibility of particles in aqueous solutions. Every DLS measurement consisted of three subsequent runs with a new sample being measured in every run and results averaged over all three runs.

Magnetic hyperthermia performance of particles was estimated by recording the temperature evolution of an aqueous suspension exposed to an AMF. The AMF was generated by a commercially available complete system (Magnetherm by Nanotherics). In this system, a water-cooled coil/capacitor-enclosure is integrated in an electric circuit containing the following elements: a function generator (GW Instek, SFG-2004), a high power radio frequency amplifier (Elektro-Automatik GmbH & Co. KG, PS 3032-20 B) and an oscilloscope (Iso-Tech, ISR 622). The circuit was driven at its resonant frequency of 524.7 kHz while the nominal magnetic field strength at the center of the 9-turn coil was approximately 24 mT (19 kA/m). An eppendorf tube containing 2 mL of 10 g/L SiO_2-coated Fe_2O_3 nanoparticle solution was inserted into the magnetic coil enclosure. The same setup was also used for release measurements. The surface temperature of the solution was regularly measured with an IR-camera (Fluke Ti110).

Composite alginate bead fabrication and characterization

Standard commercial alginate (FMC Biopolymer, Protanal LF 10/60 FT, MW ~90 kDa, M/G-ratio ~0.54) was dissolved in Milli-Q water at 1 wt % and gently stirred for 24 h. Subsequently, alginate solutions were transferred to dialysis flasks (Thermo Scientific, Slide-A-Lyzer Dialysis Flask, 3.5K MWCO) and dialyzed for 5 days. Buffer solutions (deionized water, volume 4 L) were continuously stirred and changed every 12 hours. Decreasing amounts ([30,25,20,15,7.5,0,0,0,0] g) of sodium chloride (Sigma-Aldrich, purity ≥ 99 %) were added to sustain adequate osmotic pressure levels. Upon retrieval from the dialysis flasks, alginate solutions were mixed with 20 g/L activated charcoal (Sigma-Aldrich, untreated, granular, 8-20 mesh). The charcoal was removed after 1 h using a vacuum filtration bottle (TPP "rapid"-Filtermax, 0.22 µm pore size PES-membrane). Final alginate solutions were then frozen in liquid nitrogen and lyophilized (Christ, model Alpha 2-4 LSC) resulting in the characteristic white color, in contrast to the brown color of the initial material (Supporting Information, Figure S1). Whenever storage was required, alginate powders and aqueous solutions were kept at temperatures below -18 ˚C.

To prepare precursor solutions for bead production, the flame-made nanoparticles were dispersed in 10 mL of Milli-Q water by ultrasonication (1800 s at 80 % amplitude, corresponding to ~644 kJ/L, 30/1 s pulsed). Purified alginate[41] was dissolved in 20 mL of an aqueous dextran solution. FITC-dextran with and

without an additional diethylaminoethyl (DEAE)-block (both Sigma-Aldrich, 150 kDa) was investigated. The aqueous particle suspension was then mixed with the dextran-loaded alginate solution. Alginate, particles and dextran masses were chosen to result in concentrations of 1 wt % alginate, 1 wt % SiO_2-coated Fe_2O_3 nanoparticles and 0.825 g/L dextran in the final precursor volume of 30 mL per batch. For blank batches, pure Milli-Q water was added instead of the particle suspension. Dextran was stored under inert gas atmosphere and protected from light.

Two different bead fabrication routes were examined; by vibrating nozzle technology and by manual extrusion through a syringe. For the production of beads by vibrating nozzle setup, the precursor was fed from a pressurized glass bottle (AMSI-Glass, Switzerland, 100 mL volume) which was submerged in a water bath heated to 60 ˚C. Sufficient time was granted until the precursor and the bottle reached thermal equilibrium with the water bath. The liquid precursor jet was passed through a vibrating nozzle apparatus (Inotech Encapsulator) with 400 µm inner nozzle diameter (Büchi, stainless steel) where it was mechanically broken up by the longitudinal movement superimposed onto it.[42-43] Precursor droplets were deposited in 200 mL of an aqueous 0.1 M calcium chloride dihydrate ($CaCl_2$, Sigma-Aldrich, purity ≥ 99 %) solution. The distance between nozzle and $CaCl_2$ solution surface was adjusted to 10 cm and the longitudinal vibration of the nozzle had a frequency of 1140 Hz at 80% of the maximum amplitude. After production, beads were left in the $CaCl_2$ solution for 30 min, then washed with deionized water and subsequently stored in deionized water. To determine the dextran encapsulation efficiency, representative samples of the $CaCl_2$ solution were taken for subsequent spectrophotometric analysis. All encapsulation efficiencies achieved here ranged between 40-50% for FITC-dextran and over 90 % for FITC-DEAE-dextran. Particular attention was paid to minimizing light exposure of the FITC-labeled dextrans in the precursor and the beads throughout the production process.

Alternatively, an identically prepared precursor was used to fabricate larger beads by manual extrusion from a syringe (Eppendorf Combitip plus, 5 mL) fitted with an elongated pipette tip. Due to the larger orifice diameter of the pipette tip compared to the vibrating nozzle, no precursor heating was required. All other process parameters were kept the same as in the case of the previously described vibrating nozzle apparatus.

Bead size and morphology were analyzed by optical microscopy (Zeiss Imager.M2m with AxioCam MRc). In addition to the standard halogen light source, a monochromatic Class 3B LED (Zeiss Colibri.2, 470 nm wavelength) was used to visualize dextran loading in the alginate beads. The magnetic properties of the

beads were determined by a multi-segment hysteresis loop measurement in a vibrating sample magnetometer (VSM, Princeton Measurement Corporation, MicroMag 3900) after gentle drying for 3 h at 40 ˚C and 100 mbar ambient pressure.

Release measurements

Dextran release from alginate beads was measured in water and phosphate buffered saline (PBS), at various temperatures and with and without the application of an external AMF, at sink conditions (Supporting Information, Figure S2). The fluorescence light emission of the FITC-block attached to the dextran was correlated to the dextran concentration using calibration curves (please see Supporting Information and Figure S3 for more details). Hence, a spectrophotometer (Cary Eclipse Fluorescence Spectrophotometer) or a multimode microplate reader (Tecan Infinite 200 PRO series) were used to determine prevalent dextran concentrations.

Samples for release measurements were prepared by adding 1.5 mL or 3 mL of Milli-Q water or PBS (Gibco 1X, pH 7.4) to 0.5 g of beads and then left at the respective conditions for the specified time. Prior to spectrophotometric analysis, small bead samples were centrifuged at 5.8 g for 2 min (VWR Galaxy 16 DH digital microcentrifuge) to separate the beads from the surrounding medium. No bead destruction was observed during the centrifugation process. 800 μL of the bead-free supernatant were extracted and analyzed in the spectrophotometer. For release measurements at fixed temperatures, samples were suspended in a water bath heated to the respective temperature. A heating system with an integrated temperature controller (Heidolph, MR Hei-Standard) was used to maintain constant conditions throughout the experiment.

Results and discussion

SiO_2-coated Fe_2O_3 nanoparticles

The as prepared SiO_2-coated Fe_2O_3 nanoparticles exhibit the characteristic maghemite (γ-Fe_2O_3) crystal structure with an average crystal size of 19 nm and specific surface area 77 m^2/g,[23] with excellent reproducibility (Supporting Information, Figure S4), characteristic for aerosol nanomanufacturing.[44] It should be noted that even by using a lab-scale flame reactor, gram-scale production is possible (Figure 1a, nanoparticles made from a single batch with 10.6 g/h production rate) that can easily be scaled-up for industrial plants.[36] Figure 1b shows the average hydrodynamic diameters of uncoated (circles) and SiO_2-

coated Fe_2O_3 (triangles) dispersed in water as a function of ultrasonication time at a particle concentration of 100 mg/L. The uncoated Fe_2O_3 nanoparticles form micron-sized agglomerates in water that do not break with increasing ultrasonication time (and energy). This is expected due to (i) the isoelectric point of Fe_2O_3 that lies at pH ~7 (as in the suspension here)[45] and (ii) the nanoparticle magnetic interactions that are strong enough to promote particle coupling.[37] In contrast, the hydrodynamic diameter of SiO_2-coated Fe_2O_3 nanoparticles decreases with increasing ultrasonication time reaching a plateau at 100 nm after 20 min. Therefore, the SiO_2 coating has a significant effect on minimizing particle agglomeration while it also increases the aqueous stability of these nanoparticles and facilitates their aqueous dispersion.[19] It should be noted that such hydrodynamic diameters of superparamagnetic iron oxides in aqueous suspensions are reached typically with tedious multiple-step surface functionalization processes (e.g. PEG[46], dextran[47]) further highlighting the advantages of the single-step flame synthesis and coating of nanoparticles employed here.

Figure 2 shows the temperature evolution of a ferrofluid (10 g/L) containing the SiO_2-coated Fe_2O_3 nanoparticles (23 wt% SiO_2) in the presence of an external alternating magnetic field (AMF) over time. The starting temperature is 23 ˚C and the ferrofluid exhibits a temperature increase up to 45 ˚C, characteristic of the relatively high specific absorption rate (SAR) performance of the SiO_2-coated Fe_2O_3 nanoparticles (SAR = 150 W/g for fields up to 50 kA/m).[38] The heating curve has a monotonously decreasing slope and approaches equilibrium after 2 h. It should be noted that the ferrofluid exhibits the capacity to reach clinically-relevant hyperthermia values (41-48 ˚C)[48] further highlighting the suitability of the as-prepared SiO_2-coated Fe_2O_3 nanoparticles for biomedical applications.

Multi-scale alginate composite beads

Figure 3a shows a schematic illustration of the multi-scale composite alginate hydrogel structure. The alginate hydrogel bead (light orange) contains the superparamagnetic SiO_2-coated Fe_2O_3 nanoparticles (1 wt%) and the model biomolecule (dextran) that is labeled with the FITC dye (not in scale). Therefore the resulting structure spans multiple scales of size. The bead size can be controlled by the fabrication route. We employ here two routes; (i) vibrating nozzle technology and (ii) manual extrusion through a syringe. Beads from vibrating nozzle (~800 μm) are smaller than those from manual extrusion (~2 mm). Figure 3 also shows transmission (b) and fluorescent (c) microscope images of such a multi-scale composite structure

made by vibrating nozzle setup. The bead is ~800 μm in diameter, consistent with the 400 μm nozzle employed for the bead fabrication.[49] The alginate bead appears brown in the transmission image (b) and green in the fluorescent (c) due to the presence of the SiO_2-coated Fe_2O_3 nanoparticles and the dextran-FITC, respectively. It should be noted that the nanoparticles are homogeneously dispersed within the alginate hydrogel bead even at the relatively high loading of 1 wt% due to their SiO_2 coating that renders them highly dispersible in water (Figure 1b). Alginate bead fabrication employing the bare Fe_2O_3 nanoparticles was not possible due to their large agglomerate size (Figure 1b) that resulted in the vibrating nozzle clogging. This further emphasizes the advantages of the SiO_2 coating here.

Figure 4a shows the magnetic hysteresis curves of the fabricated multi-scale structures. The presence of SiO_2-coated Fe_2O_3 nanoparticles renders the alginate beads with low coercivity near to superparamagnetic behavior. In fact, the maximum magnetization value (emu/g Fe_2O_3) is similar to that of the pure SiO_2-coated Fe_2O_3 nanoparticles at 34 emu/g,[23] indicating that the nanoparticle magnetic properties have not been altered. Figure 4b shows aqueous suspensions of the developed alginate beads (small and large) in the absence (B = 0) and presence (B > 0) of a permanent magnet. All beads localize on the side of the vial further indicating their magnetic guiding potential.

Enhanced triggered biomolecule release

The hyperthermia performance of the composite alginate hydrogel beads was also evaluated. Figure 5 shows the temperature increase of aqueous suspensions containing the superparamagnetic alginate beads in the presence of AMF as a function of time. The initial temperature was maintained at 37 ˚C, imitating *in vivo* biological conditions. The temperature of the suspension rapidly increases and reaches a plateau of 42 ˚C after 10 min. When the AMF is turned off, the temperature of the suspension gradually returns to the initial one. It should be noted that the hyperthermia temperature achieved by the beads is high enough for their employment in stimuli-responsive therapeutic applications.[7]

The potential of the composite alginate beads to be used in triggered release of biomolecules was further evaluated. Figure 6a shows the cumulative release of the DEAE-dextran-FITC from the magnetic alginate beads in PBS as a function of time for alginate suspensions incubated at 25 ˚C, 37 ˚C, 43 ˚C and in the presence of AMF with an initial temperature of 25 ˚C. The steady-state temperature in the presence of AMF reached 36 ˚C, as monitored by a thermal camera (as in Figure 5). The drug release % from alginates

depends on various parameters such as the drug molecular weight and chemical composition, cross-linking density, temperature, time.[31] The drug release values here are rather low (in the range of 1-2%), but such values are in agreement with the literature.[22,32] These drug release values are also probably attributed to the electrostatic interaction between alginate and DEAE-dextran molecules as also verified by zeta-potential measurements (Supporting Information, Figure S5). Most importantly, the release in the presence of AMF is significantly increased (>2 times) when compared to the one at 25 ˚C.[22,50] Such a two-fold increase within 2 h and especially in the case of alginate polymer beads is comparable or even better than similar magnetically triggered release of other biomolecules.[30,32] This highlights the potential of these superparamagnetic nanoparticles as a transducer element in such multi-scale structures for on-demand release of a therapeutic payload. Similar results were obtained for the dextran-FITC alginate beads in aqueous solutions (Supporting Information, Figure S6). Furthermore, Figure 6b shows the drug release data after 2 h as a function of temperature. There is a temperature dependent cumulative release with the release in the presence of AMF with a final temperature of 36 ˚C (filled symbol) right below the release achieved at 37 ˚C indicating a diffusion-driven release.[51]

It should be noted that the enhanced two-fold drug release in the presence of AMF here is demonstrated employing alginate beads. Other hydrogel systems that are temperature responsive (e.g. poly(N-isopropylacrylamide)) can achieve an optimized triggered release behavior.[5] Alginate hydrogel beads, however, are distinctive due to their high biocompatibility and facile fabrication. Furthermore, the DEAE-dextran-FITC molecules serve here as model drug and the drug release values might be different when another drug is examined. However, the triggered enhanced release will most probably be retained even in such systems. The study here also focuses on rather short-term triggered drug release by external stimuli. Nonetheless, in an organism *in vivo*, these alginate beads would eventually biodegrade, fully releasing any remaining drug in their structure. Therefore, such on-demand drug release systems are meaningful only as long as the functionality of the transducer nanofiller is preserved. Further experiments with repeating ON-OFF cycles may further provide understanding on how such a system responds to external AMF application and drug release amounts.

Conclusions

Large-scale synthesis of superparamagnetic SiO_2-coated Fe_2O_3 nanoparticles allows for detailed investigations of their potential in drug delivery biomedical systems. The suitability of flame-made, uniformly SiO_2 coated Fe_2O_3 nanoparticles as a transducer element in multi-scale architectures for on-demand drug release was validated here, liberating this field from large-scale and reproducibility-related nanomanufacture hurdles. The presence of the amorphous SiO_2 coating facilitates the aqueous dispersion of these nanoparticles and therefore their facile incorporation in the micron-sized alginate hydrogel beads without any surface functionalization with organic groups. The beads are fabricated using vibrating and/or extrusion technology and maintain the magnetic properties of the SiO_2-coated Fe_2O_3 nanoparticles. The composite multi-scale structures reach hyperthermia-relevant temperatures up to 42 ˚C in the presence of an alternating magnetic field due to the superparamagnetic nanofillers. This renders these structures suitable candidates for therapeutic applications. Upon the loading of a model biomolecule in these beads, its triggered release could be achieved by an alternate magnetic field. The cumulative release was enhanced >2 times in the presence of the alternate magnetic field (AMF). The fact that both the hyperthermia and the enhanced drug release performance of the developed system here are in agreement with the literature for similar systems[22,32,48] highlights their suitability in theranostic applications. The large-scale synthesis of such nanoparticles with high control over nanoparticle morphology and physicochemical characteristics further prompts their incorporation in smart drug delivery systems while further advancements could be realized capitalizing on multifunctional hybrid plasmonic-superparamagnetic nanoparticles[20] and temperature sensitive hydrogels[52] aiming at improved drug release performance.

Acknowledgements

This research was supported by the European Research Council under the European Union's Seventh Framework Program (FP7/2007-2013, ERC grant agreement no. 247283). Georgios A. Sotiriou was supported by a Swiss National Science Foundation *Advanced Researcher* fellowship (grant no. 145392).

References

1. J. Shi, A. R. Votruba, O. C. Farokhzad, R. Langer, *Nano Lett.,* 2010, **10**(9), 3223-3230.
2. P. Couvreur, C. Vauthier, *Pharm. Res.,* 2006, **23**(7), 1417-1450.
3. A. Jordan, R. Scholz, P. Wust, H. Schirra, T. Schiestel, H. Schmidt, R. Felix, *J. Magn. Magn. Mater.,* 1999, **194**(1-3), 185-196.

4. I. H. El-Sayed, X. H. Huang, M. A. El-Sayed, *Cancer Lett.,* 2006, **239**(1), 129-135.
5. Y. Brudno, D. J. Mooney, *J. Control. Release,* 2015, **219**, 8-17.
6. M. Bikram, A. M. Gobin, R. E. Whitmire, J. L. West, *J. Control. Release,* 2007, **123**(3), 219-227.
7. S. Mura, J. Nicolas, P. Couvreur, *Nat. Mater.,* 2013, **12**(11), 991-1003.
8. Y. H. Bae, K. Park, *J. Control. Release,* 2011, **153**(3), 198-205.
9. X. Zhu, A. F. Radovic-Moreno, J. Wu, R. Langer, J. Shi, *Nano Today,* 2014, **9**(4), 478-498.
10. D. Ling, N. Lee, T. Hyeon, *Accounts Chem. Res.,* 2015, **48**(5), 1276-1285.
11. P. D. Howes, R. Chandrawati, M. M. Stevens, *Science,* 2014, **346**(6205), 1247390.
12. D. Ling, T. Hyeon, *Small,* 2013, **9**(9-10), 1450-1466.
13. A. K. Gupta, M. Gupta, *Biomaterials,* 2005, **26**(18), 3995-4021.
14. L. H. Reddy, J. L. Arias, J. Nicolas, P. Couvreur, *Chem. Rev.,* 2012, **112**(11), 5818-5878.
15. R. E. Rosensweig, *J. Magn. Magn. Mater.,* 2002, **252**(Nov 2002), 370-374.
16. A. Jordan, R. Scholz, P. Wust, H. Fahling, R. Felix, *J. Magn. Magn. Mater.,* 1999, **201**(1-3), 413-419.
17. R. Kaiser, Miskolcz.G, *IEEE Trans. Magn.,* 1970, **MAG6**(3), 694-698.
18. B. Kozissnik, A. C. Bohorquez, J. Dobson, C. Rinaldi, *Int. J. Hyperthermia,* 2013, **29**(8), 706-714.
19. G. A. Sotiriou, A. M. Hirt, P. Y. Lozach, A. Teleki, F. Krumeich, S. E. Pratsinis, *Chem. Mater.,* 2011, **23**(7), 1985-1992.
20. G. A. Sotiriou, F. Starsich, A. Dasargyri, M. C. Wurnig, F. Krumeich, A. Boss, J.-C. Leroux, S. E. Pratsinis, *Adv. Funct. Mater.,* 2014, **24**(19), 2818-2827.
21. J. Chomoucka, J. Drbohlavova, D. Huska, V. Adam, R. Kizek, J. Hubalek, *Pharmacol. Res.,* 2010, **62**(2), 144-149.
22. S. Brule, M. Levy, C. Wilhelm, D. Letourneur, F. Gazeau, C. Menager, C. Le Visage, *Adv. Mater.,* 2011, **23**(6), 787-790.
23. A. Teleki, M. Suter, P. R. Kidambi, O. Ergeneman, F. Krumeich, B. J. Nelson, S. E. Pratsinis, *Chem. Mater.,* 2009, **21**(10), 2094-2100.
24. M. Boissiere, J. Allouche, R. Brayner, C. Chaneac, J. Livage, T. Coradin, *J. Nanosci. Nanotechnol.,* 2007, **7**(12), 4649-4654.
25. B. Mu, W. Zhong, Y. Dong, P. Du, P. Liu, *J. Biomed. Mater. Res. Part B,* 2012, **100B**(3), 825-831.
26. M. Molina, M. Asadian-Birjand, J. Balach, J. Bergueiro, E. Miceli, M. Calderon, *Chem. Soc. Rev.,* 2015, **44**(17), 6161-6186.
27. H. H. Tonnesen, J. Karlsen, *Drug Dev. Ind. Pharm.,* 2002, **28**(6), 621-630.
28. N. S. Satarkar, J. Z. Hilt, *J. Control. Release,* 2008, **130**(3), 246-251.
29. A. A. Rafi, M. Mahkam, *RSC Adv.,* 2015, **5**(6), 4628-4638.
30. S. Kondaveeti, D. R. Cornejo, D. F. S. Petri, *Colloid Surf. B-Biointerfaces,* 2016, **138**, 94-101.
31. K. Y. Lee, D. J. Mooney, *Prog. Polym. Sci.,* 2012, **37**(1), 106-126.
32. P. V. Finotelli, D. Da Silva, M. Sola-Penna, A. M. Rossi, M. Farina, L. R. Andrade, A. Y. Takeuchi, M. H. Rocha-Leao, *Colloid Surf. B-Biointerfaces,* 2010, **81**(1), 206-211.
33. A. M. Hawkins, N. S. Satarkar, J. Z. Hilt, *Pharm. Res.,* 2009, **26**(3), 667-673.

34. D. Muller-Schulte, T. Schmitz-Rode, *J. Magn. Magn. Mater.,* 2006, **302**(1), 267-271.
35. R. Mueller, L. Madler, S. E. Pratsinis, *Chem. Eng. Sci.,* 2003, **58**(10), 1969-1976.
36. K. Wegner, B. Schimmoeller, B. Thiebaut, C. Fernandez, T. N. Rao, *KONA Powder Part. J.,* 2011, (29), 251-265.
37. A. M. Hirt, G. A. Sotiriou, P. R. Kidambi, A. Teleki, *J. Appl. Phys.,* 2014, **115**(4), 044314.
38. G. A. Sotiriou, M. A. Visbal-Onufrak, A. Teleki, E. J. Juan, A. M. Hirt, S. E. Pratsinis, C. Rinaldi, *Chem. Mater.,* 2013, **25**(22), 4603-4612.
39. A. Teleki, B. Buesser, M. C. Heine, F. Krumeich, M. K. Akhtar, S. E. Pratsinis, *Ind. Eng. Chem. Res.,* 2009, **48**(1), 85-92.
40. A. Teleki, M. C. Heine, F. Krumeich, M. K. Akhtar, S. E. Pratsinis, *Langmuir,* 2008, **24**(21), 12553-12558.
41. S. Fusco, M. S. Sakar, S. Kennedy, C. Peters, R. Bottani, F. Starsich, A. Mao, G. A. Sotiriou, S. Pane, S. E. Pratsinis, D. Mooney, B. J. Nelson, *Adv. Mater.,* 2014, **26**(6), 952-957.
42. D. B. Seifert, J. A. Phillips, *Biotechnol. Prog.,* 1997, **13**(5), 562-568.
43. D. Serp, E. Cantana, C. Heinzen, U. von Stockar, I. W. Marison, *Biotechnol. Bioeng.,* 2000, **70**(1), 41-53.
44. S. E. Pratsinis, *AIChE J.,* 2010, **56**(12), 3028-3035.
45. S. Yu, G. M. Chow, *J. Mater. Chem.,* 2004, **14**(18), 2781-2786.
46. M. D. Butterworth, L. Illum, S. S. Davis, *Colloid Surf. A-Physicochem. Eng. Asp.,* 2001, **179**(1), 93-102.
47. S. Mornet, J. Portier, E. Duguet, *J. Magn. Magn. Mater.,* 2005, **293**(1), 127-134.
48. A. Singh, S. K. Sahoo, *Drug Discov. Today,* 2014, **19**(4), 474-481.
49. M. Whelehan, I. W. Marison, *J. Microencapsul.,* 2011, **28**(8), 669-688.
50. X. Hua, S. Tan, H. M. H. N. Bandara, Y. Fu, S. Liu, H. D. C. Smyth, *PLoS One,* 2014, **9**(12), e114271.
51. P. L. Ritger, N. A. Peppas, *J. Control. Release,* 1987, **5**(1), 37-42.
52. J. Shi, N. M. Alves, J. F. Mano, *Macromol. Biosci.,* 2006, **6**(5), 358-363.

Figure captions

Figure 1. (a) Digital photograph of SiO_2-coated Fe_2O_3 nanoparticles made from a single batch in a lab-scale reactor. (b) Average hydrodynamic diameter of uncoated (red circles) and SiO_2-coated Fe_2O_3 (blue triangles) dispersed in water as a function of ultrasonication time at a particle concentration 100 mg/L. Note the break in the ordinate. The error bars correspond to the standard deviation of at least 3 measurements (error bars are smaller than the symbols for the blue triangles).

Figure 2. The temperature increase of aqueous suspension with 10 g/L of SiO_2-coated Fe_2O_3 nanoparticles (ferrofluid) in the presence of an alternating magnetic field, exhibiting the hyperthermia potential of these nanoparticles.

Figure 3. (a) Schematic illustration of the multi-scale structure developed in this study. The alginate bead (gray) contains the superparamagnetic SiO_2-coated Fe_2O_3 nanoparticles (1 wt%, blue-brown particles) and the model biomolecule (dextran, green dots) that is labeled with the FITC dye (not in scale). Transmission (b) and fluorescent (c) optical microscope images of such a bead.

Figure 4. (a) Magnetic hysteresis curves of the developed multi-scale structures. (b) Digital photographs of an aqueous suspension of the developed alginate beads in the absence and presence of a permanent magnet.

Figure 5. Temperature increase of aqueous suspensions containing the magnetic alginate beads in the presence of an alternating magnetic field (AMF) as a function of time. The inset shows an image of the thermal camera that is used to monitor the temperature of the suspension.

Figure 6. Cumulative release of DEAE-dextran-FITC from the superparamagnetic alginate beads in PBS as a function of time for suspensions incubated at 25 (blue circles), 37 ˚C (green triangles), 43 ˚C (brown squares) and in the presence of an alternating magnetic field (AMF, filled red diamonds) with initial temperature of 25 ˚C. The steady-state temperature in the presence of AMF reached 36 ˚C. Power law equation fits of each profile are shown with broken lines. Error bars correspond to standard deviation of three measurements. The cumulative release in the presence of AMF is enhanced > 2 times in comparison to the control (25 ˚C). (b) Drug release values after 2 h for all samples. The drug release increases with increasing temperature.

Figures

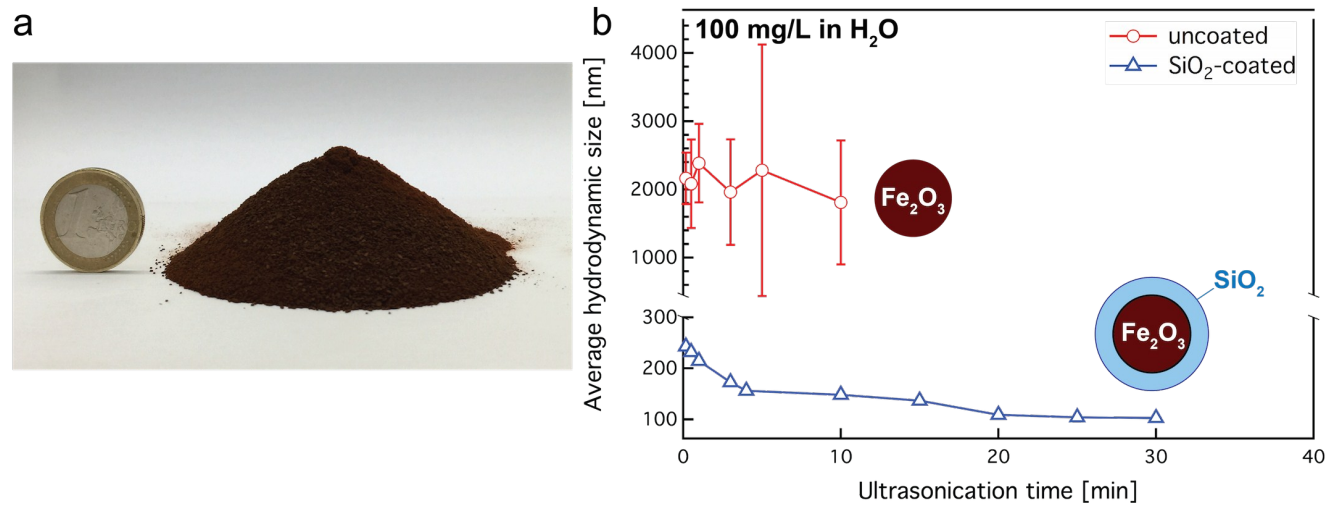

Figure 1

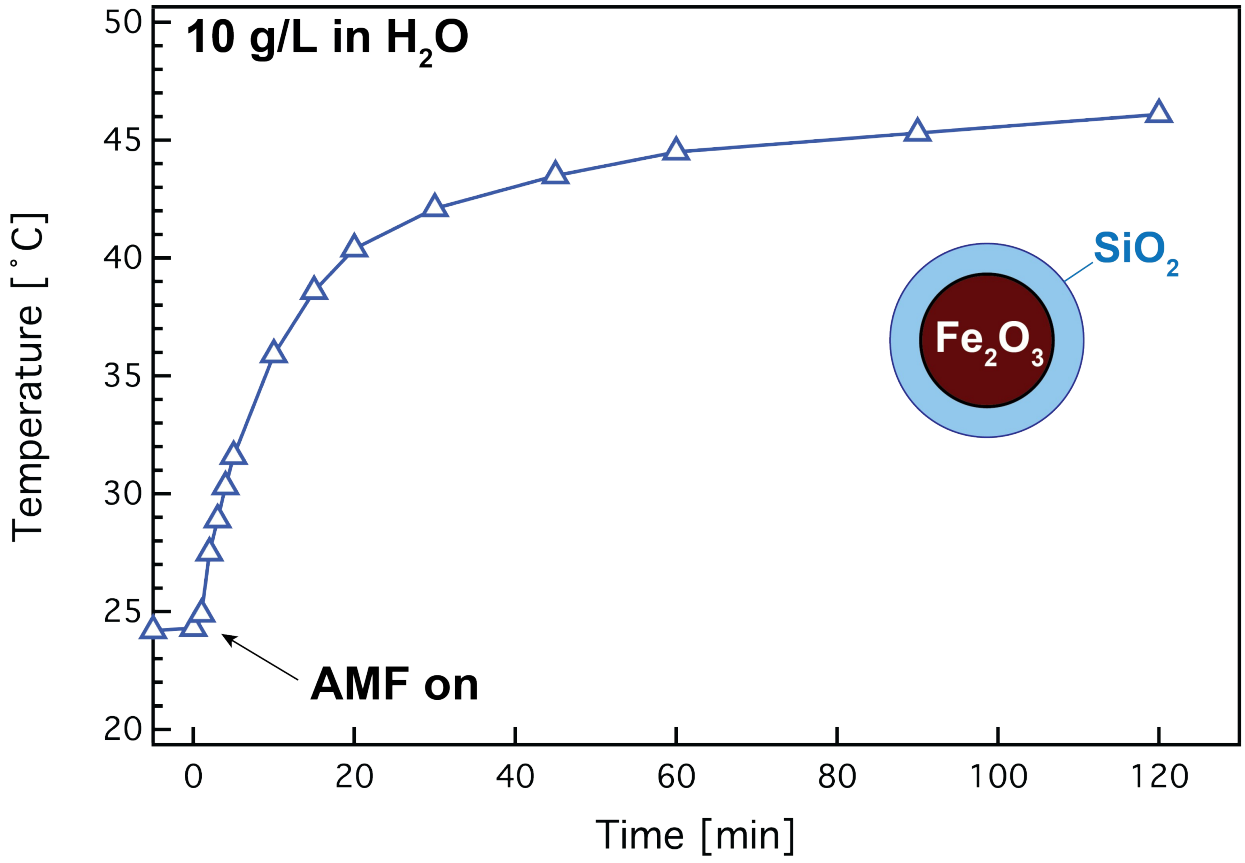

Figure 2

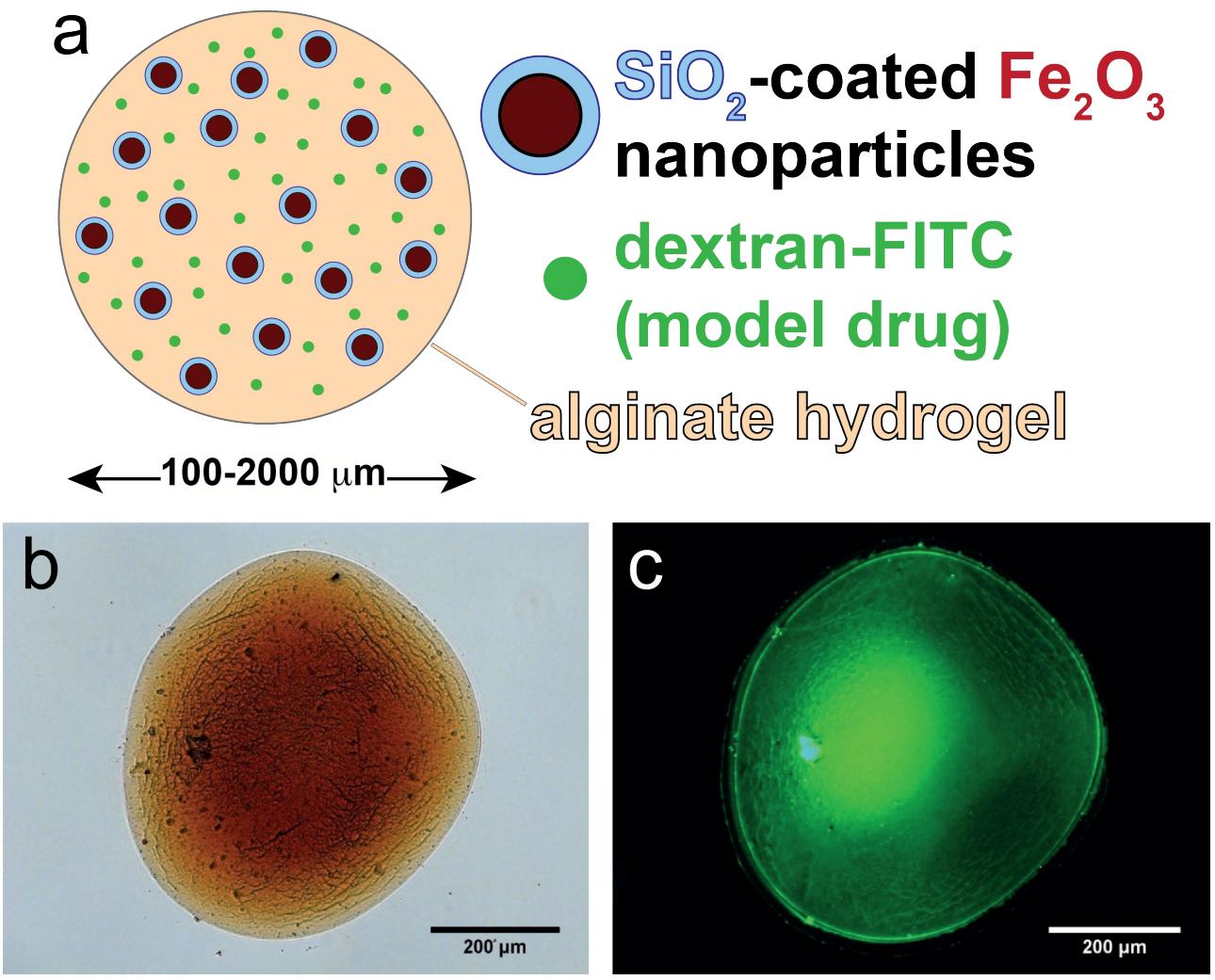

Figure 3

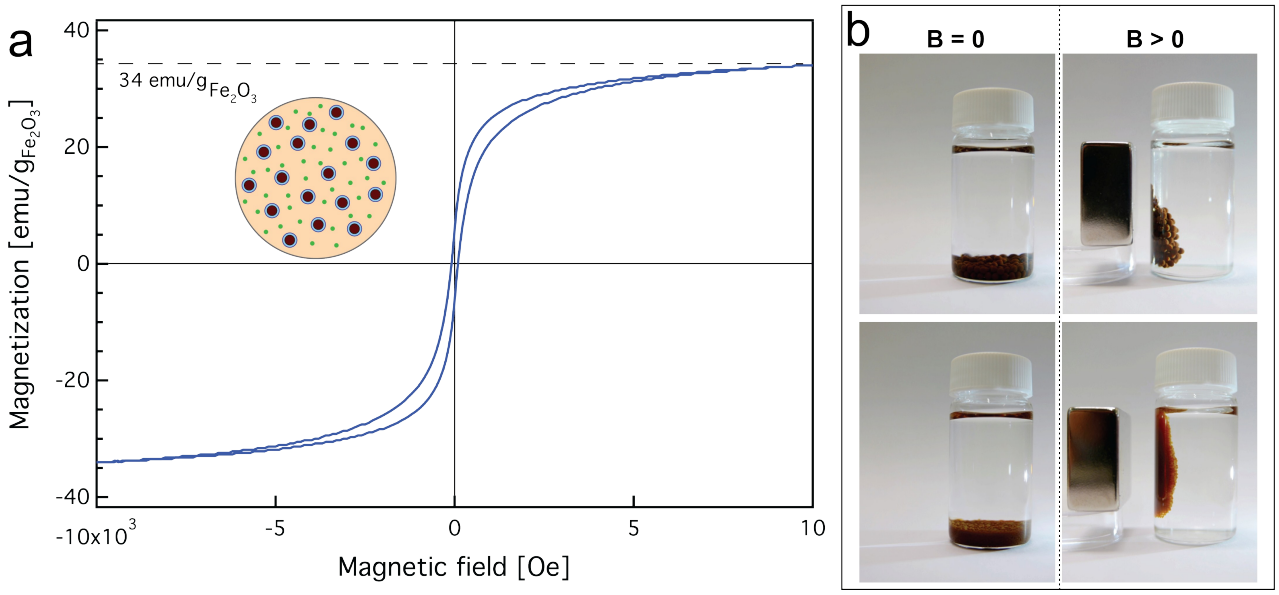

Figure 4

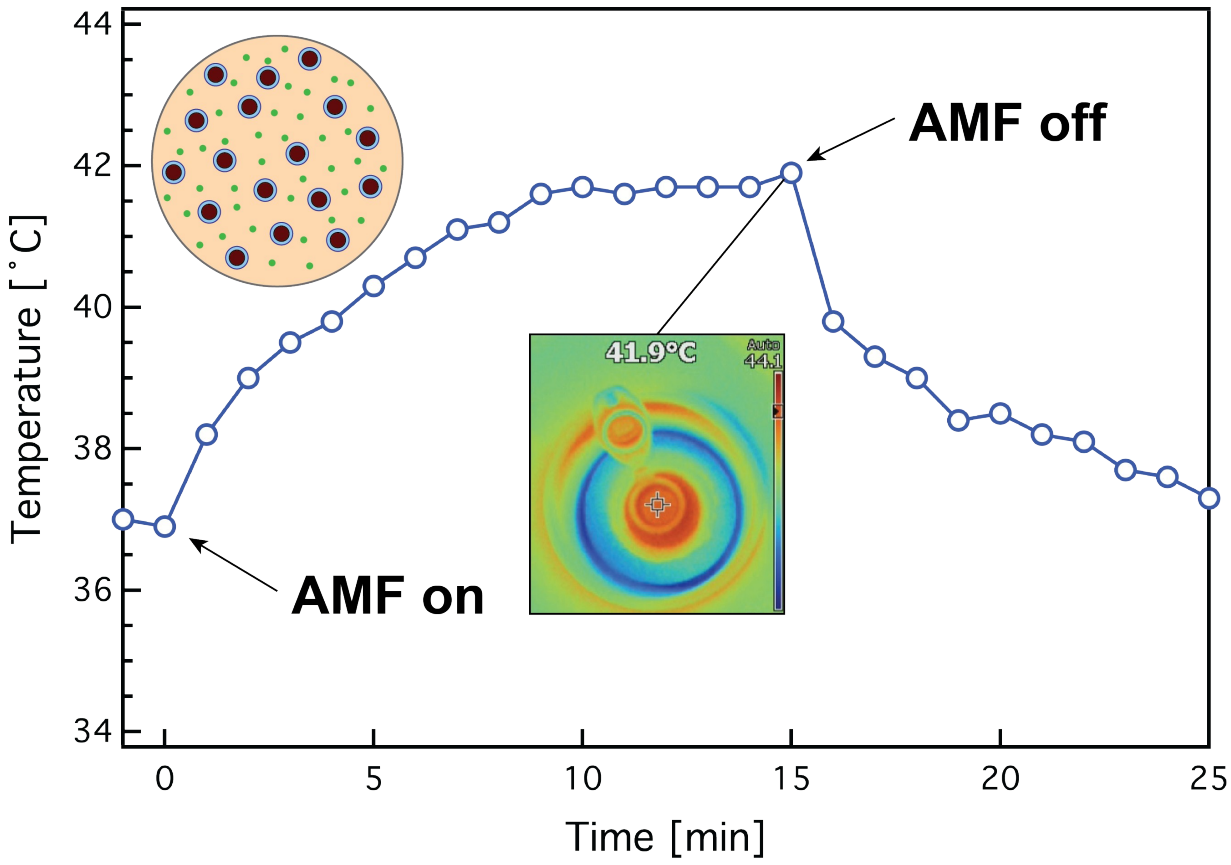

Figure 5

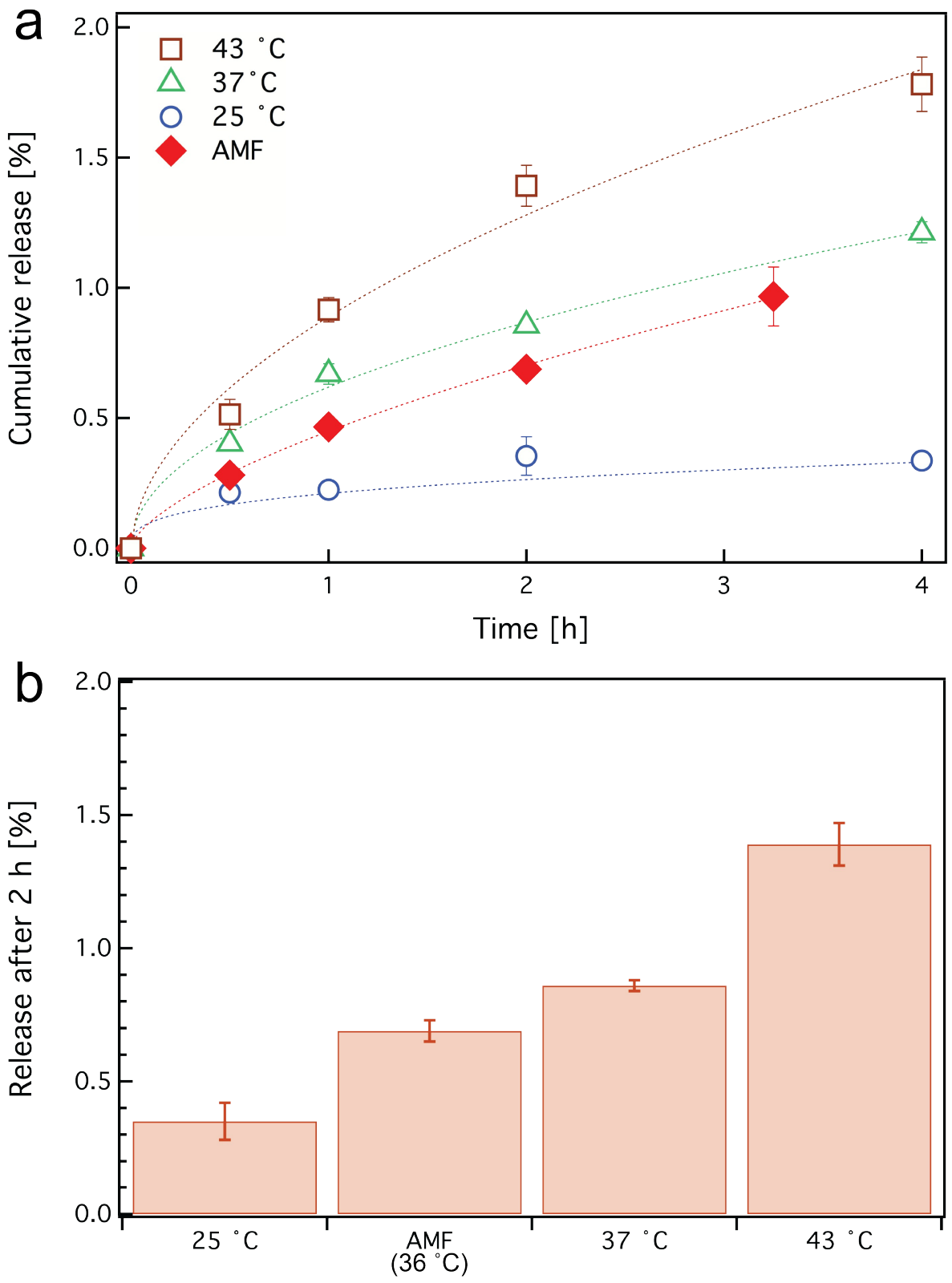

Figure 6